RESEARCH ARTICLE

Shape recovery properties and load-carrying capacity of a 4D printed thick-walled kirigami-inspired honeycomb structure

Chengbin Yue[1] · Wei Zhao[1] · Fengfeng Li[1] · Liwu Liu[1] · Yanju Liu[1] · Jinsong Leng[2]

Abstract

Kirigami arts have provided a more promising method for building multiscale structures, which can shape two-dimensional (2D) sheets into three-dimensional (3D) configurations by cutting and folding. Here, we first carried out a theoretical analysis of the mechanical properties of 2D honeycomb lattice structures and experimental verification combined with finite element (FE) simulation. Furthermore, a series of thick-walled 3D kirigami-inspired honeycomb (TW3KH) structures with different mechanical properties were designed and fabricated on the exploration and optimization of geometric parameters of 2D honeycomb structures. The investigations of folding feasibility, self-expansion, and self-folding performance experimentally showed that our designed four-dimensional (4D) printing structure had good programmability and shape memory capability and a large volume change ratio during shape change. Meanwhile, research on its compression deformation behavior found that the TW3KH structures can recover load-bearing capacity very well when the angle is positive. Therefore, these TW3KH structures have great advantages in space-saving smart load-bearing equipment.

Graphic abstract
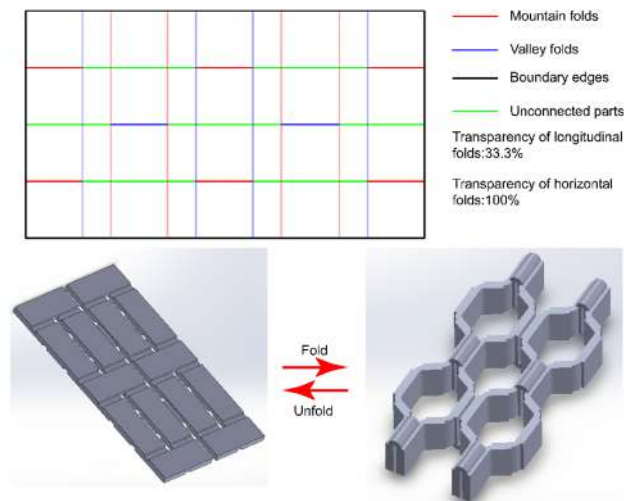
Keywords Shape memory · 4D printing · Kirigami arts · Pattern transformation

---

Chengbin Yue and Wei Zhao have contributed equally to this work.

✉ Liwu Liu
liulw@hit.edu.cn

✉ Jinsong Leng
lengjs@hit.edu.cn

[1] Department of Astronautical Science and Mechanics, Harbin Institute of Technology, Harbin 150001, China

[2] Center for Composite Materials and Structure, Harbin Institute of Technology, Harbin 150080, China

Introduction

The honeycomb structure is derived from the honeycomb in nature [1, 2]. It is a structure composed of regular hexagonal single rooms with all the rooms facing down or facing one side and symmetrically arranged back to back [3]. It is known for its high specific stiffness/strength [4, 5] and energy absorption capacity [6–9], which has inspired the attention of many researchers and has been extensively used in aerospace, transportation packaging, architecture load-bearing, and medical implant fields [10–15]. However, once manufactured, its structure will not be changed according to the needs of the application, which greatly limits its applications in some special application scenarios, especially in smart space deployable structures with load-bearing requirements. Four-dimensional (4D) printing technology is more flexible for manufacturing complex structures [16–18]. In addition, it allows the preparation of objects with reprogramming properties that can return to their original shape in response to external stimuli due to the property of shape memory polymers (SMPs) [19–21]. It is expected to improve its flexibility and adaptability in applications.

In recent years, the art of kirigami, which has more degrees of freedom than origami, has provided a more promising method for building multiscale structures, which can shape two-dimensional (2D) sheets into three-dimensional (3D) configurations by cutting and folding [22–26]. Kirigami-inspired energy-absorbing structures [27], programmable multistable metamaterials [28], pluripotent materials [29], bifurcated stents [30], deployable mirror/solar panels [31], soft robotics [32], morphing components [33], and multiscale structures [34] have been developed. However, the complexity of the kirigami principle and the need for an active configuration usually results in many inconveniences before practical application. Fortunately, some recent reports of 4D printing technology combined with origami structures have brought us some new inspiration. Tao et al. [35] prepared an origami metamaterial using the 4D printing method combined with SMP and developed its theoretical deformation model. The prepared origami structure exhibited controlled twist deformation under compressive loads as well as shape programming and self-expanding properties. Meanwhile, its mechanical properties can be controlled by the temperature, and the translation between monostable and bistable can be accomplished by adjusting the parameters. Liu et al. [36] designed laminated Miura-origami structures and fabricated them with 4D printing technology. Furthermore, the application as an actuator was demonstrated under compressive loading. Xin et al. [37] developed an origami structure with a honeycomb core, which has enhanced stiffness and shape recovery force. Meanwhile, its potential application in space deployable structures was validated.

To the best of our knowledge, although much research on 4D-printed origami structures has been conducted, most scholars mainly focus on their self-expanding function, and it may also be meaningful to explore the application of 4D-printed thick-walled kirigami-inspired structures using their self-folding function in space-saving load-bearing structures.

In this paper, we first built an analytical model of the structure under the conditions of considering viscoelastic deformation and designed a 2D hexagonal lattice structure with different topological angles. The effects of each topological angle on the equivalent elastic modulus (E) and Poisson's ratio (v) were predicted and analyzed by this model. The finite element (FE) and experimental results were in good agreement with the theoretical prediction. Based on the exploration and optimization of the geometric parameters of the 2D honeycomb structure, we designed and fabricated a series of thick-walled 3D kirigami-inspired honeycomb (TW3KH) structures used by fused deposition modeling (FDM) technology. Furthermore, the programmability and shape recovery performance were evaluated by investigating the folding feasibility, self-expansion, and self-folding of the structure. We simulated the shape recovery process of vertically programmed structures using ABAQUS software via the generalized Maxwell viscoelastic constitutive model (GMM). Finally, we investigated the differences in the load-bearing performance of the structure before and after shape recovery through compression experiments.

Theory and design

Design and theoretical analysis of the 2D lattice structure

Figure S1 (Supplementary Information) shows the geometric parameters of the 2D hexagonal honeycomb structure unit cell in general, where h is the length of the straight side, l is the length of the hypotenuse, and m and a are the in-plane and out-plane thicknesses of the honeycomb, respectively. The ratio of the in-wall thickness to the hypotenuse is 0.1, and θ is the angle between the hypotenuse and the horizontal. Both positive Poisson's ratio and negative Poisson's honeycomb are considered, so their variation range is $\left(-\frac{1}{3}\pi, \frac{1}{3}\pi\right)$.

A coordinate system is established in Fig. S2 (Supplementary Information). The material of a monolithic honeycomb structure is regarded as a uniform, continuous, and orthotropic material. In the calculation process, we approximate the inner wall of the honeycomb as a Timoshenko beam, and the shear deformation and stretch deformation of the inner walls are considered. Then, the equivalent E and v are
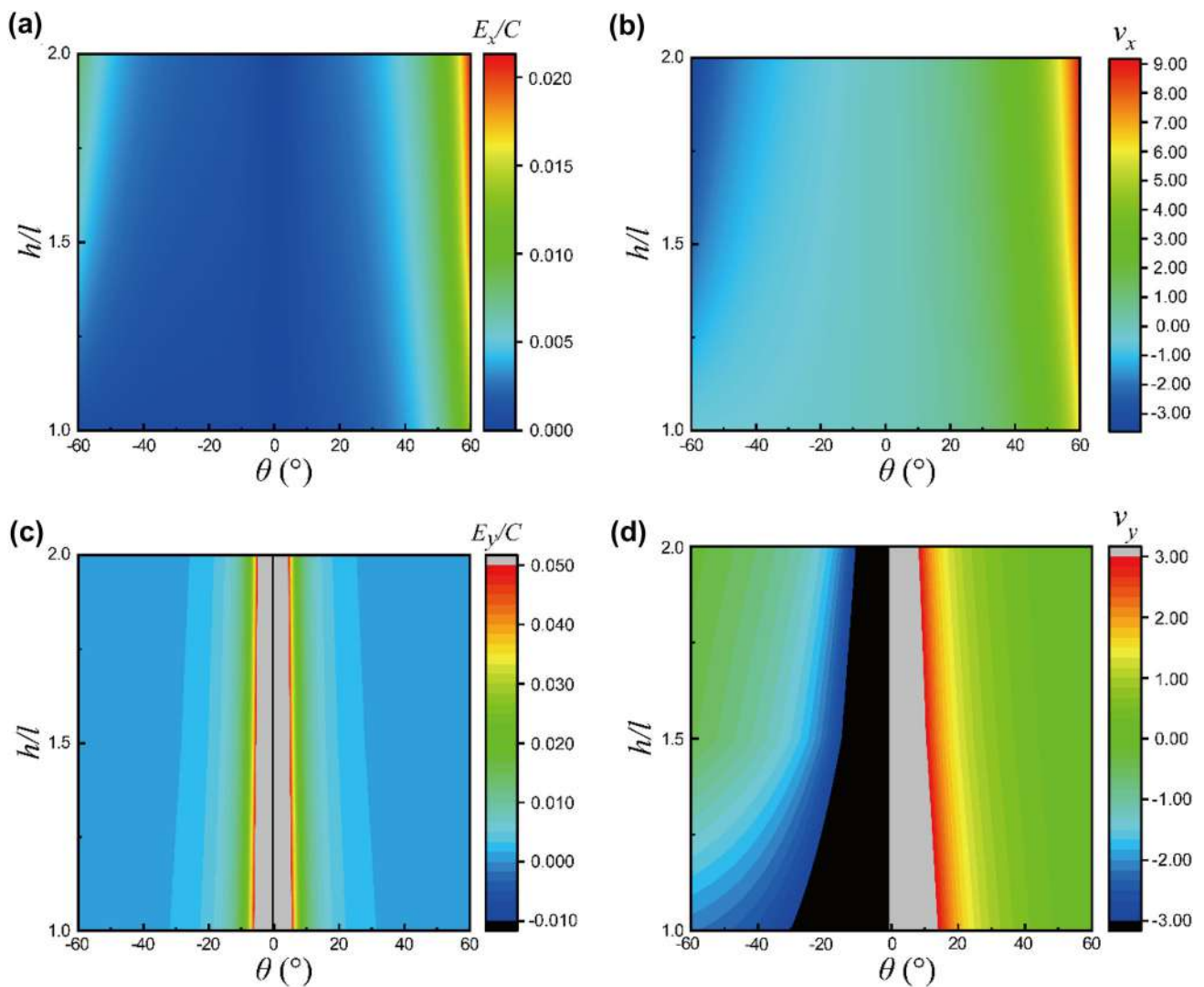
Fig. 1 Information of geometrical parameters θ and h/l on the equivalent E and v of the hexagonal honeycomb structure in the x- and y-directions: **a** E_x/C; **b** v_x; **c** E_y/C; **d** v_y

calculated in the x- and y-direction of the structure, respectively.

Based on the prediction model obtained in Supplementary Information S1, we discuss the effects of geometrical parameters θ and h/l on the equivalent E and v of the 2D hexagonal honeycomb structure in the x- and y-directions, respectively. As illustrated in Fig. 1, the change in the angle θ has a great influence on the equivalent E and v in both directions. The magnitude of this effect becomes greater upon increasing the value h/l in the x-direction. Similarly, the changed value h/l also plays a pivotal role in the process of changing Poisson's ratio v_y in the y-direction with the angle θ; however, the effect on the equivalent elastic modulus E_y/C is weak (C is the Young's modulus of viscoelastic constituent material in Supplementary Information S1). Therefore, to adjust the modulus and Poisson's ratio of structures over a wider range, we choose hexagonal honeycombs with a ratio of the straight side h to the hypotenuse l of 2 for the experimental and FE simulation investigations in the following work.

Design of the 4D printed TW3KH structure

Based on the inspiration of kirigami arts and the 2D honeycomb lattice structure in Sect. Design and theoretical analysis of the 2D lattice structure, we designed a printable TW3KH structure with different Poisson's ratios. First, the kirigami-based origami principle with the TW3KH structure of $\theta=30°$ as an example is shown in Fig. 2a. The red, blue, black, and green strokes represent mountain folds, valley folds, boundary edges, and unconnected parts, respectively. The final fold angle of a mountain or valley crease depended on its opacity. For example, 100%=180° (fully folded), 50%=90°, and 0%=0° (flat). All folding angles between 0° and 180° can be considered. Furthermore, the bidirectional

Fig. 2 Bidirectional deformable thick-walled 3D kirigami-inspired honeycomb (TW3KH) model ($\theta = 30°$): **a** schematic illustration of the kirigami-based origami principle; **b** geometric definitions and 2D pattern of the TW3KH structure; **c** geometric definitions and 3D pattern of the TW3KH structure
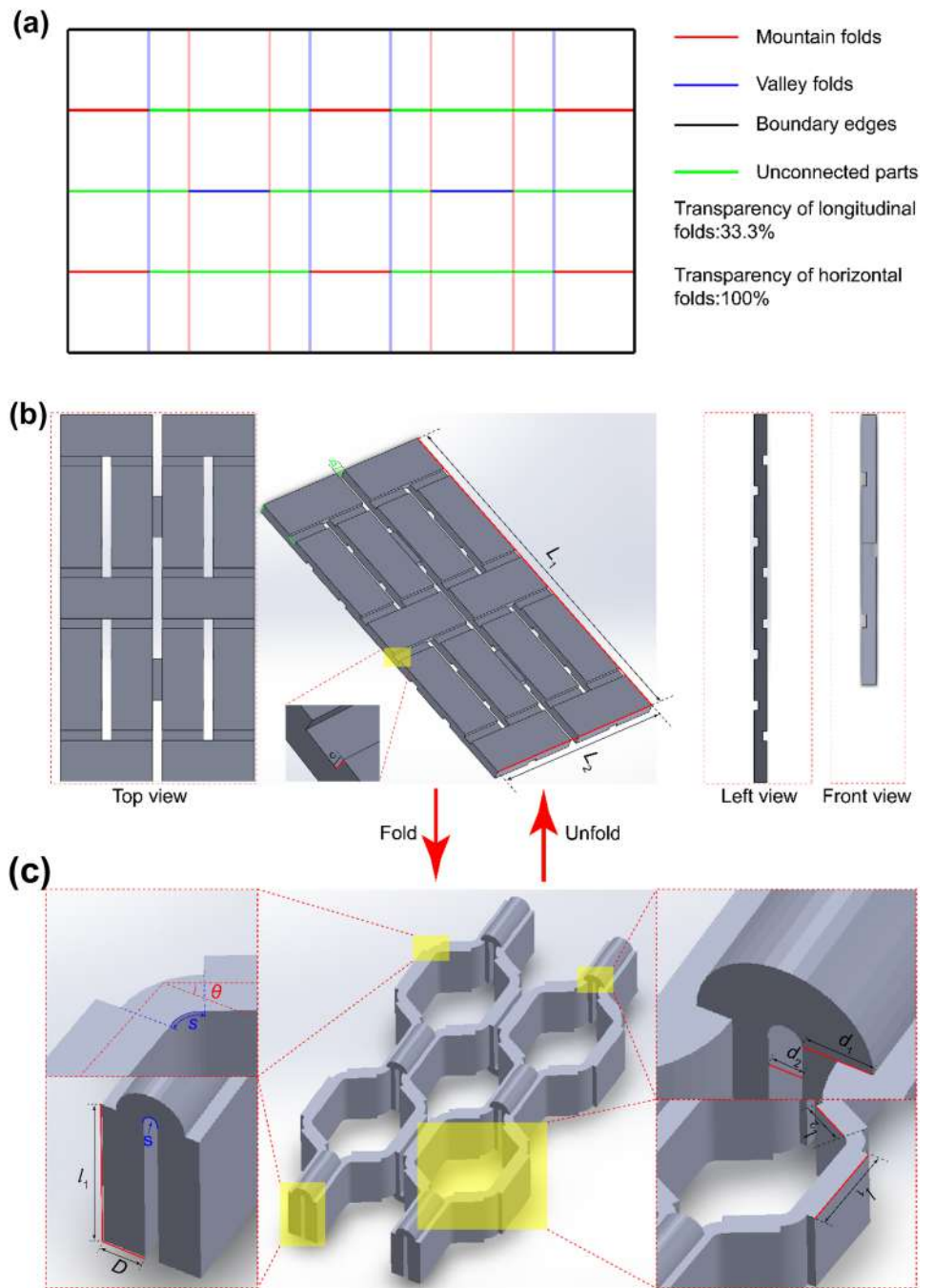
Table 1 Geometric parameters of the thick-walled 3D kirigami-inspired honeycomb (TW3KH) structures in the unfolding and folding states

Parameter	Unfolding state				Folding state						
	L_1	L_2	b	c	l_1	l_2	D	d_1	d_2	S	θ
Value (mm)	133.8	70.8	3.6	2.4	15	7.5	3.6	3.6	1.146	1.2	$\left(-\frac{\pi}{3}, \frac{\pi}{3}\right)$

deformable TW3KH model was designed. Figures 2b and 2c show the geometric definitions of the TW3KH structure ($\theta = 30°$) in the 2D and 3D patterns corresponding to the

parameters in Fig. S1a (Supplementary Information). The kirigami model of the 2D pattern comprises panels and fold gaps (corresponding to fold), and the kirigami model of the

3D pattern comprises horizontal panels, inclined panels, and hinges (corresponding to fold). The specific parameters of the model are listed in Table 1.

Materials and methods

Materials and specimen fabrication

The polylactic acid (PLA) filament with shape memory properties used in FDM was obtained from Shenzhen Guanghua Weiye Co., Ltd. (China). The elastic modulus of PLA material is 2–3 GPa, and the glass transition temperature is 60–65 °C. Here, we first prepared dumbbell-shaped tensile specimens according to the ASTMD638 standard and tensile specimens of hexagonal honeycomb structures with different angles. The dimensions of the honeycomb specimen are as follows: straight side h=16 mm, hypotenuse l=8 mm, honeycomb in-wall thickness m=0.8 mm, and specimen out-wall thickness a=0.8 mm; the included angle θ is $\pm60°$, $\pm40°$, and $\pm20°$. Since the hexagonal honeycomb structure is orthotropic, tensile specimens in two directions need to be prepared for each angle specimen. The 2D digital image correlation (DIC) technique was used for the measurement of Poisson's ratios of the 2D hexagonal honeycomb structures. To enhance the grayscale matching properties, black and white paint was sprayed on the surface of the measured structure as speckles. In addition, 2D and 3D TW3KH structures with different Poisson's ratios were fabricated. The addition picture for the honeycomb structure folded by paper, the printed 2D lattice structure, and the TW3KH structures is shown in Fig. S3 (Supplementary Information). After measurement, we found that the folded honeycomb structure can hold hundreds of times its own weight, and the size of the 4D printed specimen was the same as that of the actual modeling.

In this experiment, a Vertix 3D printer with a nozzle size of 0.2 mm was used to print the test specimens. The printing temperature was set to 200 °C, and the printing speed was set to 30 mm/s. The layer thickness was 0.2 mm, and the filling density was 100%.

Uniaxial tensile and relaxation testing

The uniaxial tensile test was conducted on a Zwick-010 universal testing machine to study the variation in the elastic modulus of the PLA dumbbell-shaped tensile specimens with temperature. The test temperature was 25–75 °C, and the step size was 5 °C. Before the experiment, the sample was stabilized for 15 min at the proper temperature. Subsequently, a deformation was applied to the specimen with a loading rate of 1 mm/min. In addition, the mechanical properties of 2D honeycomb lattices printed from PLA filaments were tested at room temperature.

The relaxation properties of PLA at different temperatures were investigated on a Zwick-010 universal testing machine with a temperature-controlled cabinet. The test temperature range was 25–75 °C. A deformation of 1 mm was applied at a speed of 1.5 mm/min and maintained for 1800 s. Stress history was recorded over time.

Shape recovery behavior characterization and FE method

Shape memory programming and recovery experiments of TW3KH structures were performed in hot water and an oven, respectively. First, the flat TW3KH structure was placed in hot water at 90 °C and folded into two kinds of 3D target shapes. Then, the target temporary shape was fixed at a temperature of approximately 25 °C. Finally, the shape recovery experiment from 3D to 2D was performed in hot water at 90 °C, and the shape recovery process was recorded using a digital camera. Similarly, the reverse programming and shape recovery experiments of the TW3KH structures were performed in hot water at 90 °C. Here, the shape-fixing ability of all samples was excellent in the shape memory test, so only their shape recovery rate was measured using the image processing software ImageJ. The measurement method is shown in Fig. S4 (Supplementary Information). The shape recovery rate of structure is:

$$R_{\mathrm{r}} = \frac{R_{\mathrm{r}}(\mathrm{left}) + R_{\mathrm{r}}(\mathrm{right})}{2},$$

where $R_{\mathrm{r}}(\mathrm{left}) = \frac{180° - \theta_{\mathrm{left}}}{180°}$, $R_{\mathrm{r}}(\mathrm{right}) = \frac{180° - \theta_{\mathrm{right}}}{180°}$. Each sample was measured five times. In addition, to compare the influence of the temperature environment on the shape recovery property, we carried out shape recovery experiments of the TW3KH structures with θ=30° in an oven at 90 °C.

In particular, the TW3KH structures with θ=30° were compressed by a certain displacement in the vertical direction in an oven at 90 °C. The shape recovery experiment was performed after fixing the temporary shape, and the shape recovery process was recorded. The FE simulation of its shape memory behavior was performed using the commercial software ABAQUS. We assumed that the material is isotropic and viscoelastic during the FE simulation. Eight-node hexahedral linear-reduced integration elements (C3D8R) were used to mesh the model of the TW3KH structures with different angles. In our work, the classical viscoelastic theory (GMM) was used to describe the deformation behavior of the TW3KH structures of SMP by referring to the method in the work of Song et al. [38]. The SMP constitutive model and related parameters
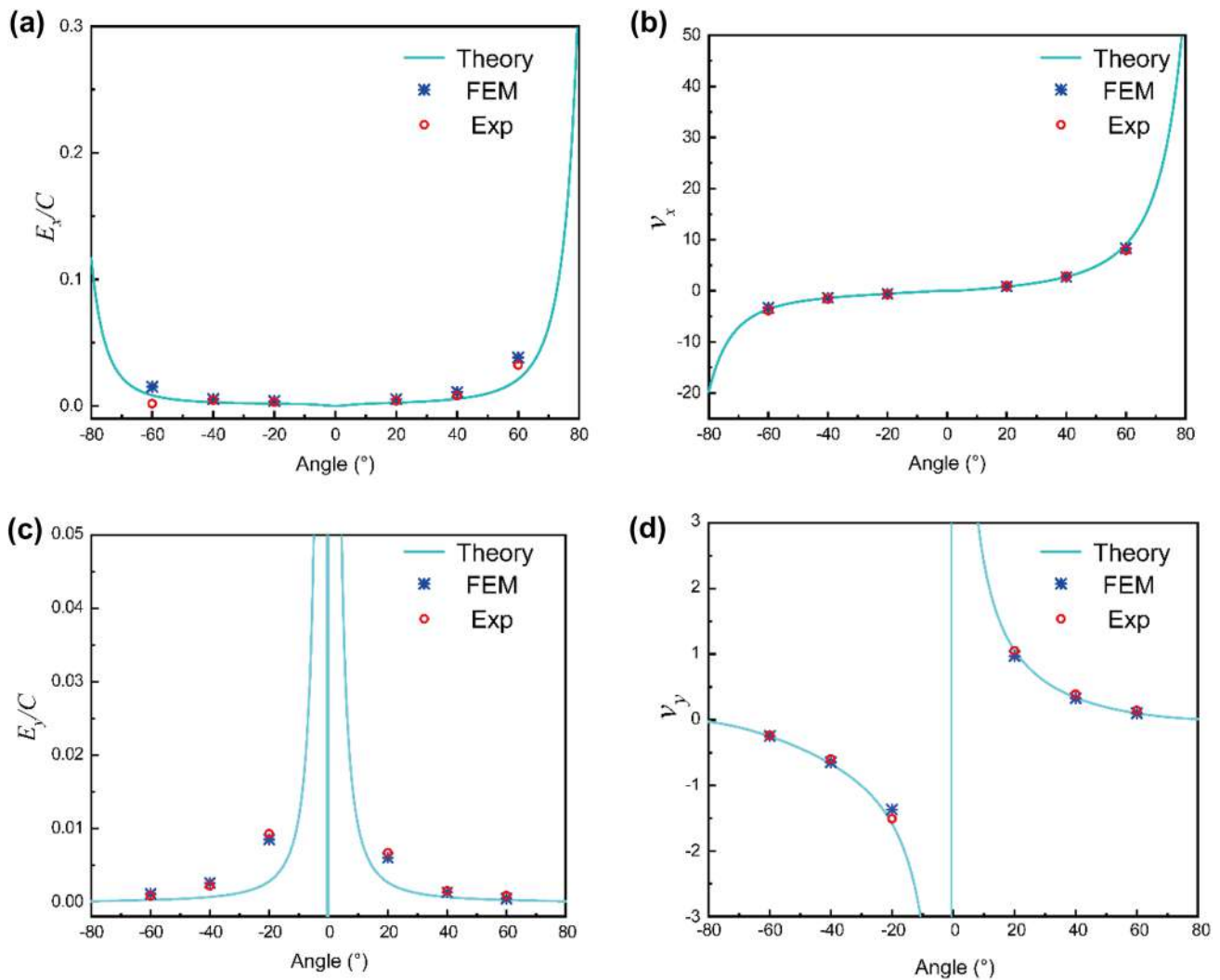
Fig. 3 Effect of geometric parameters θ on the mechanical property of 2D honeycomb structures: **a** equivalent elastic modulus E_x/C in the x-direction; **b** Poisson's ratio v_x in the x-direction; **c** equivalent elastic modulus E_y/C in the y-direction; **d** Poisson's ratio v_y in the y-direction (FEM: finite element method; Exp: experiment)

can be found in detail in Table S1 (Supplementary Information). The Poisson's ratio of the material was set as 0.39.

## Compression tests and FE method

The load-bearing behavior of the TW3KH structure was measured by quasi-static compressive tests under environmental conditions using an electronic general mechanical tester. A preloading loading rate of 0.5 mm/min and a normal loading rate of 5 mm/min were applied to ensure the quasi-static process. Moreover, the quasi-static compressive response of the TW3KH structures was simulated by the explicit dynamic algorithm using the commercial FE software ABAQUS. The elastic–plastic constitutive model was

used. Similarly, eight-node hexahedral linear-reduced integration elements (C3D8R) were used to mesh the model of the TW3KH structures with a different angle.

Results and discussion

Mechanical properties of 2D hexagonal honeycomb structures

The influence of geometric parameters θ on the mechanical properties of hexagonal honeycomb is studied. Figure 3 shows the comparison diagram of the theoretical value, simulation value, and experimental value of equivalent E and equivalent v in two directions (x and y) for different types of hexagonal honeycomb structures, and the experimental
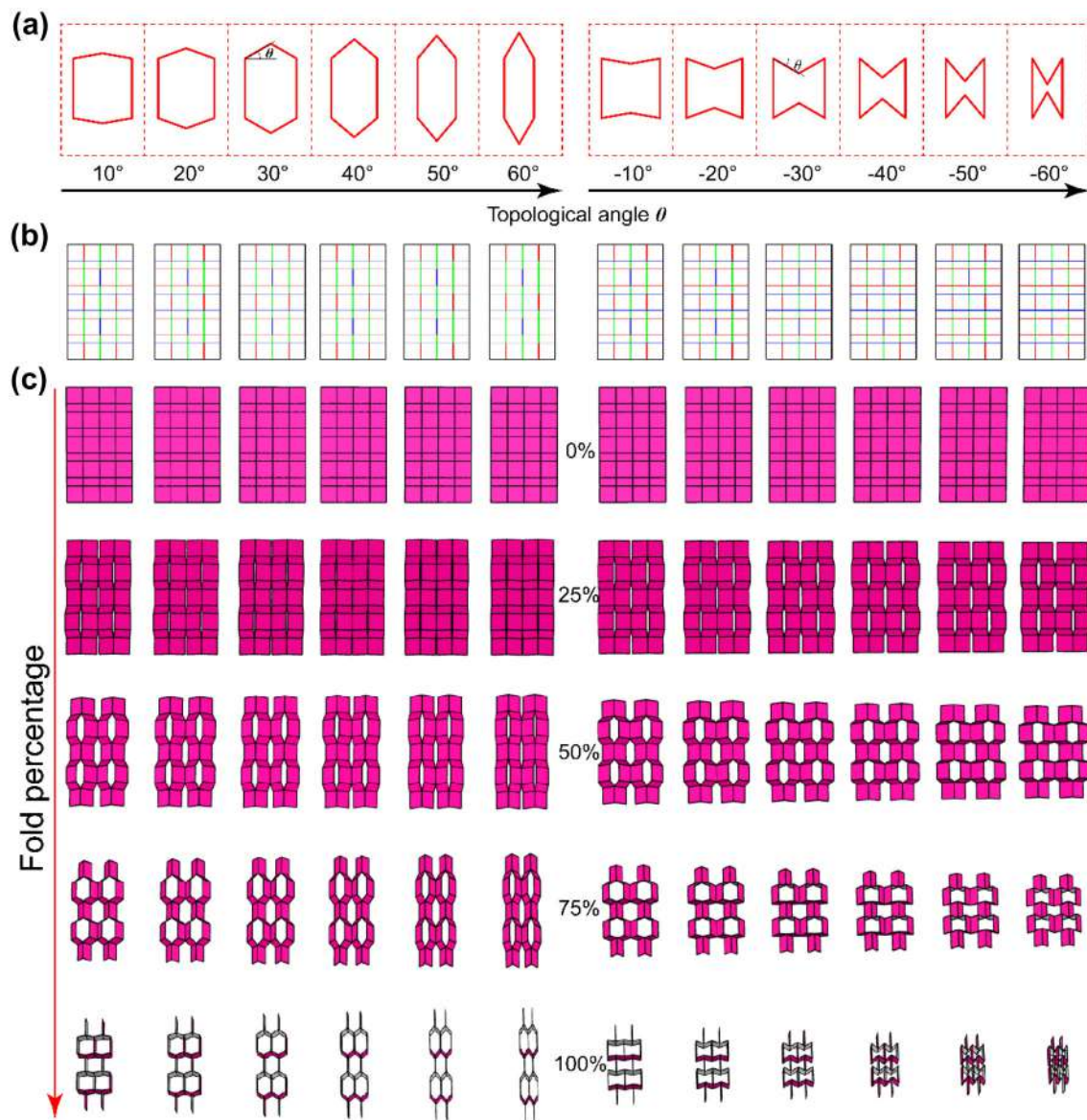
Fig. 4 Self-folding process of the flat panels: **a** 2D lattice cell unit with different angles; **b** corresponding crease picture with different transparencies of the transverse creases; **c** 3D honeycomb structures with different fold percentages in the self-folding process

model is shown in Fig. S3d (Supplementary Information). The simulation value and experimental value are very close to the theoretical value. Meanwhile, the functional relationship between the simulation and experimental values of equivalent E and v with the angle θ has good consistency with the theory. Moreover, as seen in the theoretical value curve, the equivalent E and v of the hexagonal honeycomb structure in the x-direction increase upon increasing the absolute value of the angle θ. The equivalent E in the y-direction decreases with increasing absolute value of the angle θ. When the angle θ is approximately $\pm 10°$, the v in the y-direction will change greatly with the angle θ. Therefore, when designing a deformable honeycomb structure using 4D printing

technology, we can use the above theoretical formula to predict the equivalent E and v of the structure.

Self-folding of 2D kirigami

Inspired by deformable 2D honeycomb structures and kirigami-inspired origami principles, we design a self-folding 2D kirigami crease picture (Fig. 4b) with different transparencies of horizontal creases corresponding to different angles θ in Fig. 4a. Figure 4c shows the self-folding process from flat panel to 3D honeycomb structures with different fold percentages (0%, 25%, 50%, 75%, 100%). As the folding percentage gradually increases, the flat panels
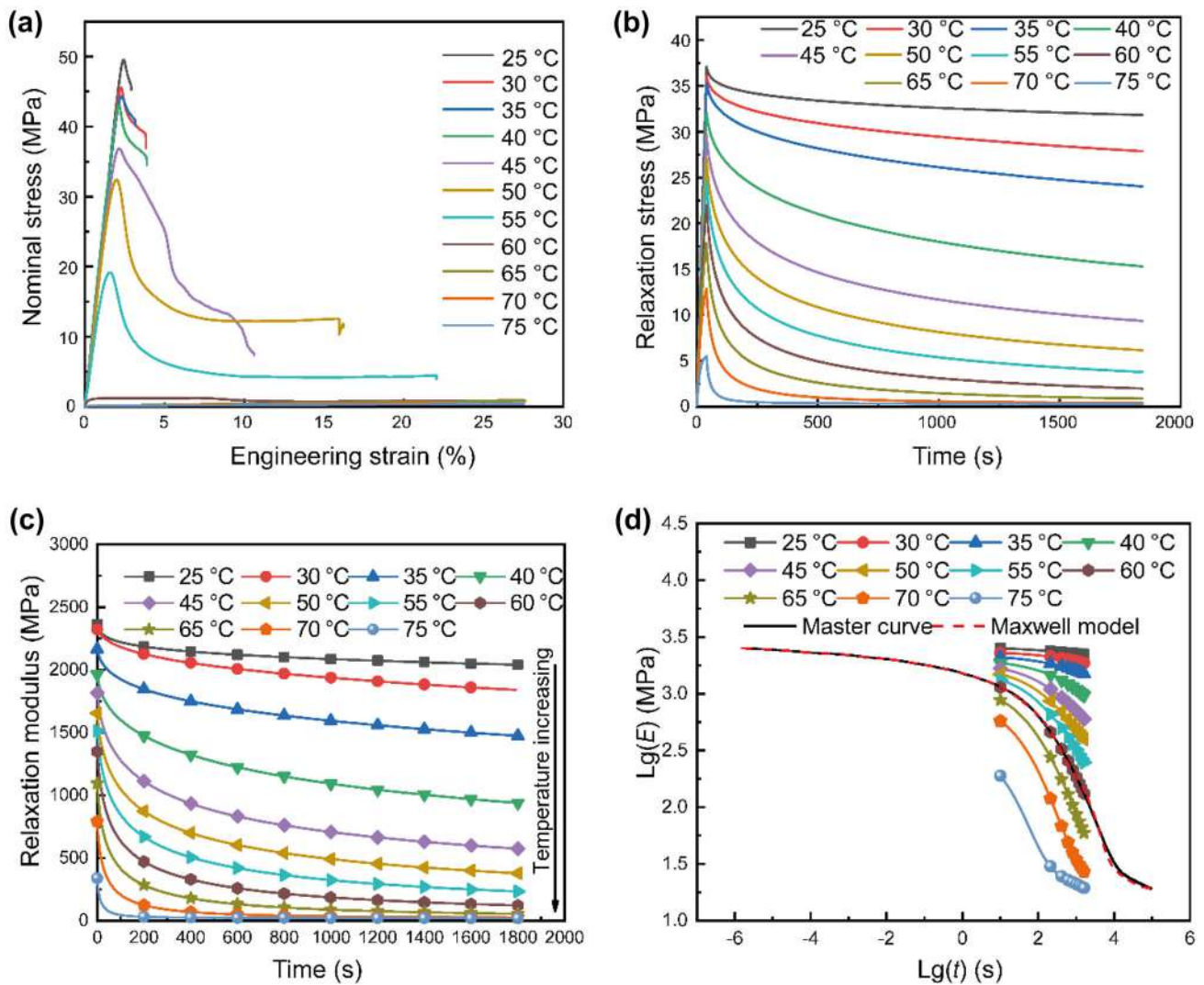
Fig. 5 Mechanical properties of shape memory polymer (SMP) polylactic acid (PLA) at various temperatures: **a** the isothermal uniaxial tensile stress–strain curves at 11 different temperatures; **b** stress relaxation behavior; **c** the curves of relaxation modulus vs time; **d** experiment and model comparison of the PLA relaxation master curve at $T_{\mathrm{ref}} = 60$ °C over a wide temperature range according to the time–temperature equivalence principle

with different lateral transparency creases eventually self-fold into 3D kirigami honeycomb structures corresponding to 2D honeycomb structures with different angles θ. This is because different creases in transparency correspond to different folding angles in the kirigami principle. Similar to the 2D honeycomb structure, these self-folding 3D honeycomb structures with different angles will also produce different equivalent elastic moduli and Poisson's ratios under tension or compression.

Uniaxial stretching and relaxation behavior of SMP PLA

To better understand the mechanical properties of materials and obtain the parameters required for shape memory FE simulation, we conduct the isothermal uniaxial tensile test and relaxation experiments of SMP PLA at 11 different temperatures [39, 40]. The isothermal uniaxial tensile stress–strain curves under 11 different temperatures are displayed in Fig. 5a. It can be observed that the PLA specimens have a large elongation at high temperatures and exhibit brittle fracture at low temperatures during the tensile process. In addition, the elastic modulus of PLA gradually decreases with increasing temperature, which illustrates the variable stiffness properties of PLA. At the same time, this feature implies that shape memory programming is feasible. It is especially noteworthy that the elastic modulus of PLA exhibits a cliff-like decline at approximately 60 °C, which is of great significance to the selection of programming temperature. After calculation, we obtain that the elastic modulus
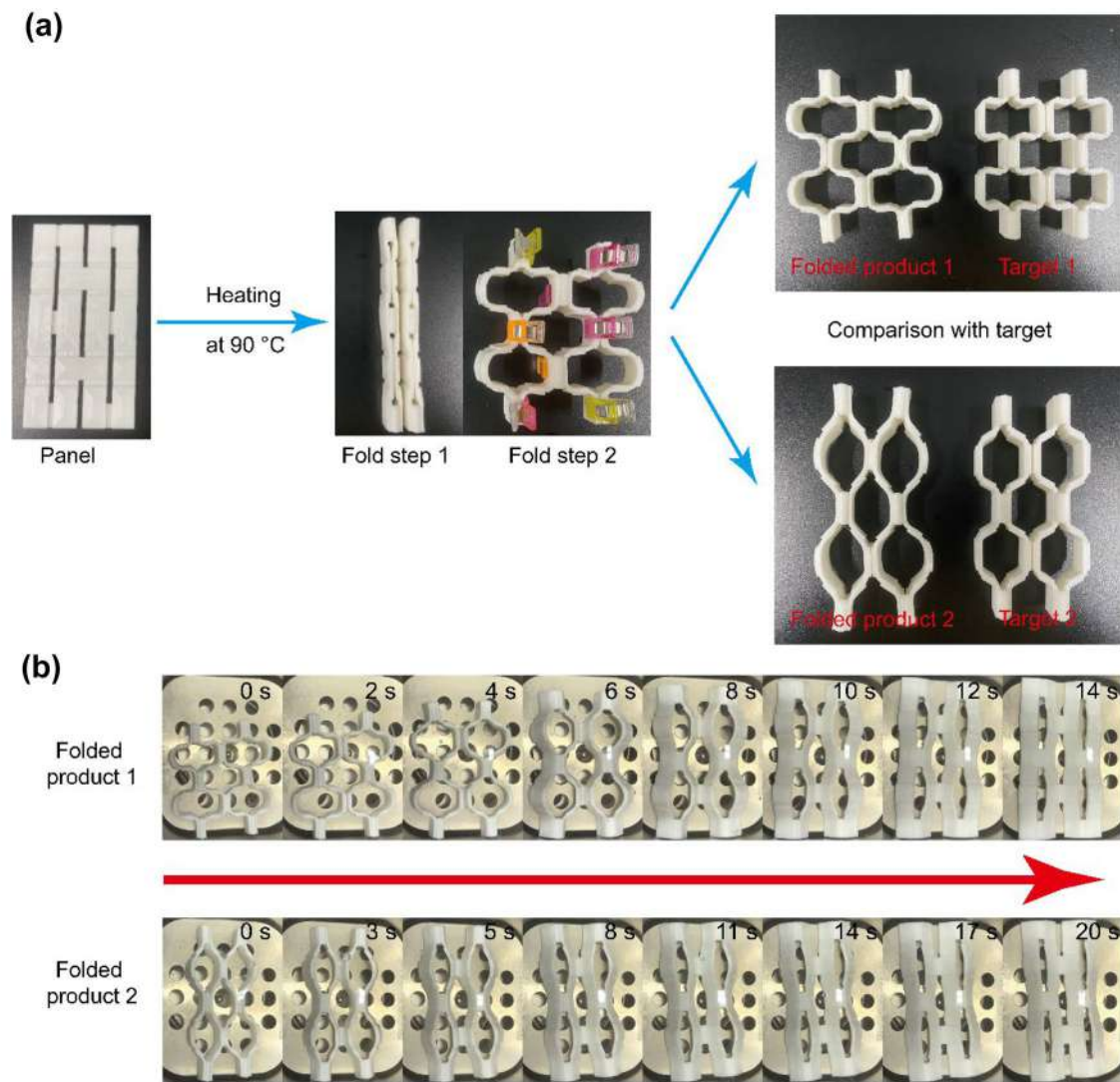
Fig. 6 a Folding process of the flat panel. **b** Self-expanding process of two kinds of folded thick-walled 3D kirigami-inspired honeycomb (TW3KH) structures

of PLA is ~2.1 GPa, the strength is ~49 MPa, and the elongation is ~2.9% at 25 °C. Figures 5b and 5c show the curves of relaxation stress vs. time and relaxation modulus vs. time, respectively. It is observed that the influence of temperature and time on the varied history of relaxation stress and relaxation modulus is particularly obvious. The relaxation stress and modulus gradually decrease and level off upon increasing the temperature. The initial relaxation modulus of PLA at 25 and 75 °C are 2.36 GPa and 331.83 MPa, respectively. Then, the classic generalized Maxwell constitutive model was used for the description of the viscoelastic behavior of SMP PLA (Supplementary Information S3). As shown in Fig. 5d, the relaxation master curve of SMP PLA at the reference temperature is obtained by using the time–temperature equivalence principle and the relaxation curves measured experimentally

at different temperatures. The master curve is in good qualitative agreement with the Maxwell model curve.

Folding and self-expanding feasibility verification

The variable stiffness properties of SMP give flat panels the ability to be foldable into the target shape, and the shape memory effect makes folded TW3KH structures self-expandable. Figures 6a and 6b show the folding process of the flat panel and the self-expansion process of two kinds of folded TW3KH structures, respectively. It can be seen that the flat panel is folded into two kinds of target shapes by fold steps 1 and 2 in water at 90 °C. The shape of the folded product is similar to the shape of the target, but the details are imprecise. This is due to the low modulus of the

Fig. 7 a Programable process of self-folding thick-walled 3D kirigami-inspired honeycomb (TW3KH) structures. **b** Self-folding process from flat panel to TW3KH structures in hot water. **c** Shape recovery demonstration of the TW3KH structures with θ of 30° in the oven
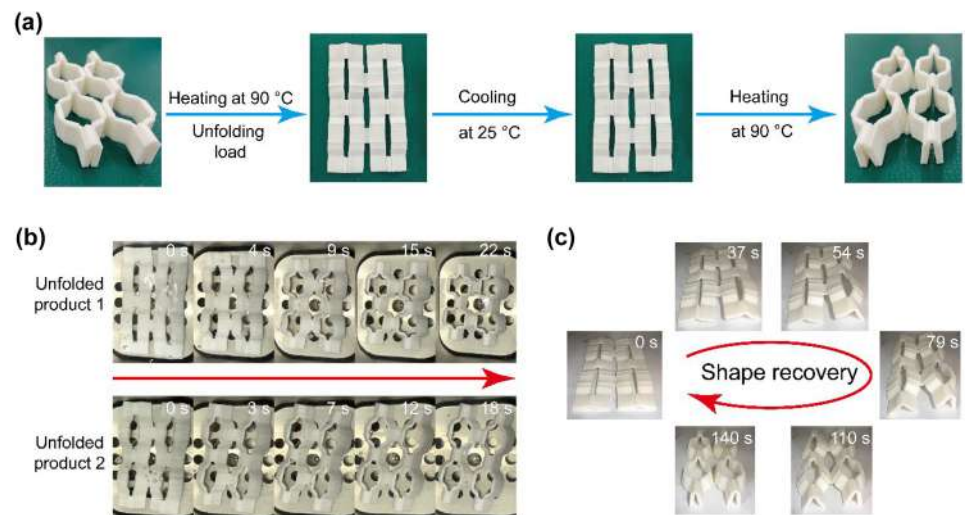
material in hot water and the presence of restoring forces during the folding process, which makes the complex folding process difficult to precisely control. Then, we conducted the shape recovery experiment of folded products. Figure 6b shows that folded products 1 and 2 recover from the folded TW3KH structures to the flat panel in hot water at 90 °C within 14 and 20 s, respectively. The shape recovery rate of folded product 1 was faster than that of folded product 2. This is mainly due to more internal stress caused by large programming deformation during programming. This kind of thick-walled flat panel structure capable of large deformation shaping and self-expanding under thermal stimulation may find a wide range of applications in the field of space deployable structures.

Self-folding and shape recovery rate of TW3KH structures

Compared with the self-expansion of folded TW3KH structures, the self-folding from the flat structure to the TW3KH structures may have more practical usefulness in more applications, such as space-saving load-bearing structures. To understand the potential of our structure for this application, we perform shape recovery experiments, shape recovery rate statistics, and volume change rate statistics. Figure 7 shows the programmable process of the self-folding TW3KH structure and the self-folding process of flat panels. As shown in Fig. 7a, the printed TW3KH structure is first programmed into a flat panel shape at a temperature of 90 °C under the unfolding load. Then, the flat temporary shape is fixed at

room temperature. Finally, the shape recovery process in hot water and the oven at 90 °C are displayed in Figs. 7b and 7c, respectively. It can be seen that unfolded products 1 and 2 complete the self-folding process in 22 and 18 s, respectively. Furthermore, Fig. 7c shows that the shape recovery time of unfolded product 2 is 140 s in the oven at 90 °C, which is longer than that in hot water. This is mainly because the heat transfer rate in the hot water is greater than that in the oven.

To understand the space-saving application of the self-folding TW3KH structures, their shape recovery data and volume change rate data of TW3KH structures from the 3D pattern to the 2D pattern are summarized in Table 2. The shape recovery data demonstrate that when $\theta > -20°$, the TW3KH structures have good shape memory properties, whose shape recovery rate is above 80%. In contrast to the self-folding process of TW3KH structures with $\theta > 0°$, the change in the shape recovery force during the self-folding process of TW3KH structures with $\theta < 0°$ is more complicated. It should be noted that when θ is negative, the shape recovery rate gradually decreases upon increasing its absolute value. The possible reasons are that the shape recovery forces at the hinges of the TW3KH structures partially cancel each other out during the complex self-folding process. Furthermore, the volume change ratio illustrates the excellent space-saving capability of the TW3KH structures. The highest volume change ratio of TW3KH structures from the 3D pattern to the 2D pattern is up to 435% in all samples. It can be concluded that the TW3KH structures have very promising applications in space-saving transportation.

Table 2 Shape recovery data of self-folding thick-walled 3D kirigami-inspired honeycomb (TW3KH) structures and volume change data of TW3KH structures from the 3D pattern to the 2D pattern

| Geometric parameter θ	−60°	−50°	−40°	−30°	−20°	−10°	10°	20°	30°	40°	50°	60°
Shape recovery rate (%)	66.5±2.7	70.3±1.9	73.1±2	75.7±0.4	76.7±0.4	81.1±0.5	80.5±0.3	80.9±0.4	82.7±0.3	81.8±0.4	85.3±0.5	84.1±0.4
Volume change ratio (%)	253	291	329	364	395	418	435	426	406	375	335	287

Comparison between experiment and simulation of the shape recovery process

An FE simulation of the shape recovery process of the TW3KH structures programmed in the vertical direction is carried out with the commercial software ABAQUS, and the relevant model parameters are given in Table S1 (Supplementary Information). The four analysis steps during the thermomechanical cycle simulation are set up as follows: First, the structure is compressed with a displacement of 30 mm at a high temperature of 90 °C, leading to the structural angle changing from positive to negative. Second, the temperature field is changed from 90 to 25 °C while maintaining the displacement. Third, the external load is removed at low temperatures. Finally, the structure is reheated to 90 °C under zero load. An experimental and simulation comparison of the programming and shape recovery processes of 30° TW3KH structures in the vertical direction is shown in Fig. 8. According to the results of experiments and simulations, it can be seen that the SMP TW3KH structures recover their original shape under temperature stimulation, and the structural angle changes from a negative value back to a positive value. It is obvious that the shape memory performance of the structure programmed in the vertical direction is better compared to the folding and unfolding programming. Therefore, the SMP TW3KH structures are capable of realizing programmable functions and automatic unfolding.

Bearing behavior of the TW3KH structures

To study the compressive deformation behavior of the TW3KH structures and the load-bearing capacity before and after shape recovery, we perform compression experiments and FE simulations. Figure 9 shows the compression force–displacement curves of TW3KH structures before (I) and after (II) shape recovery. When the structure angle θ is positive, the compressive stiffness of the original structure increases upon increasing the angle, which is similar to the theory of the 2D honeycomb structure. The reason is that the force form at the hinge of the structure gradually changes from bending to compression as the angle increases during the compression process. Meanwhile, the stiffness of all shape-recovered structures is greater than that of the original structure due to the presence of incomplete shape recovery angles. Neither shows a distinct stage of densification. Out-60-II prematurely exhibits compression instability. As shown in Fig. S6 (Supplementary Information), the simulated deformation of the original structure is in good qualitative agreement with the experimental observations. When the structure angle θ is negative, the densification phase of the original structure during compression can be observed. The structure enters the densification stage earlier upon decreasing the angle, which can also be confirmed in experimental

Fig. 8 Experiment and simulation comparison of programming and shape recovery processes of 30° thick-walled 3D kirigami-inspired honeycomb (TW3KH) structures in the vertical direction (FEM: finite element method; EXP: experiment)
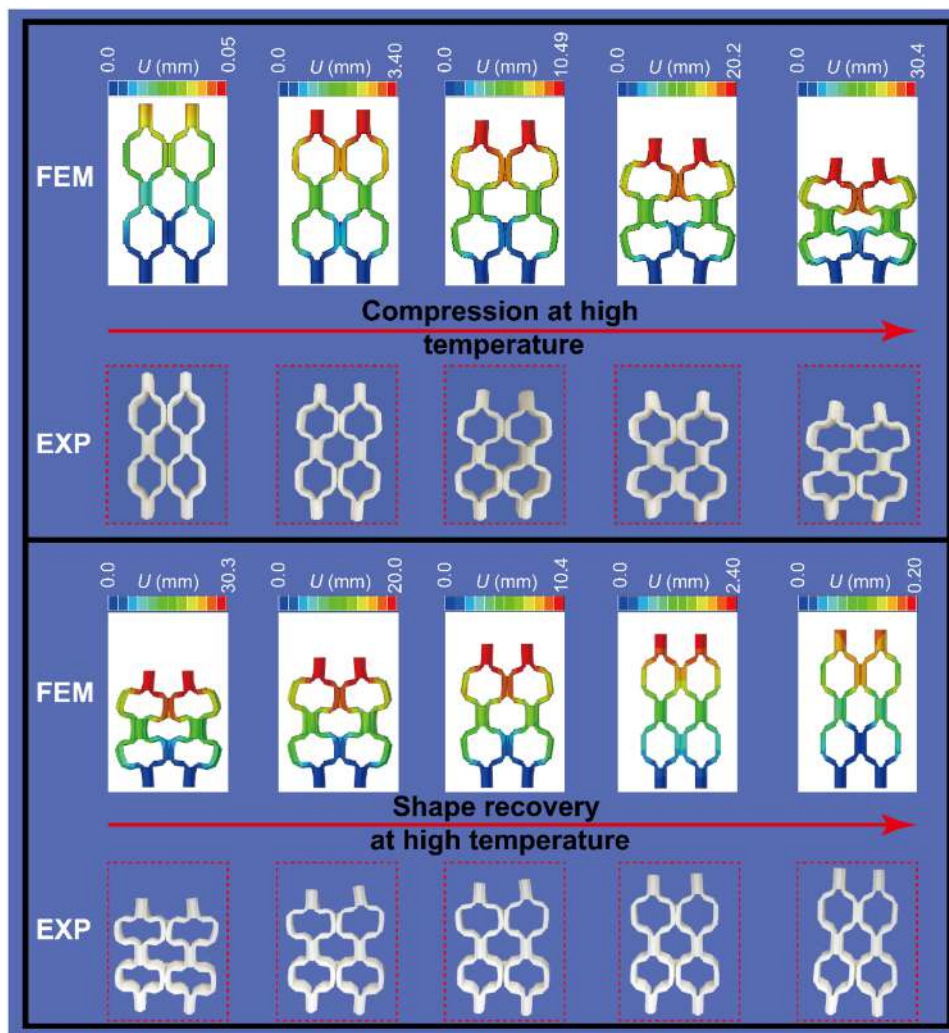

observations and FE simulations (Fig. S6 in Supplementary Information). However, the TW3KH structure after shape recovery did not recover its load-carrying capacity well. This is mainly because when the structure angle is negative, the shape recovery rate of the structure is too small, resulting in a large difference in the structure before and after shape recovery, resulting in different deformation trends.

Conclusions

In this work, we obtained the equivalent E and v of 2D honeycomb structures through theoretical calculations and verified them through experiments combined with FE simulations. The results showed that the experimental and simulation

results were in good agreement with the theoretical values. After optimizing the geometric parameters, we further designed a TW3KH structure inspired by kirigami principles and 2D honeycomb structures. Its folding feasibility, self-expanding, and self-folding performance were experimentally studied. The structure had good programmability and shape memory capability and a large volume change ratio during shape change. Experiments and simulations of the shape recovery process of structures programmed in the vertical direction illustrated that the programmed TW3KH structure can recover from concave to convex shapes under transition temperature stimulation. The compression experiments showed that the geometric parameters θ had a significant effect on the load-bearing capacity of the structure, and imperfect shape recovery had little effect on its load-carrying properties and even had a positive effect when the angle was positive. In conclusion, the designed
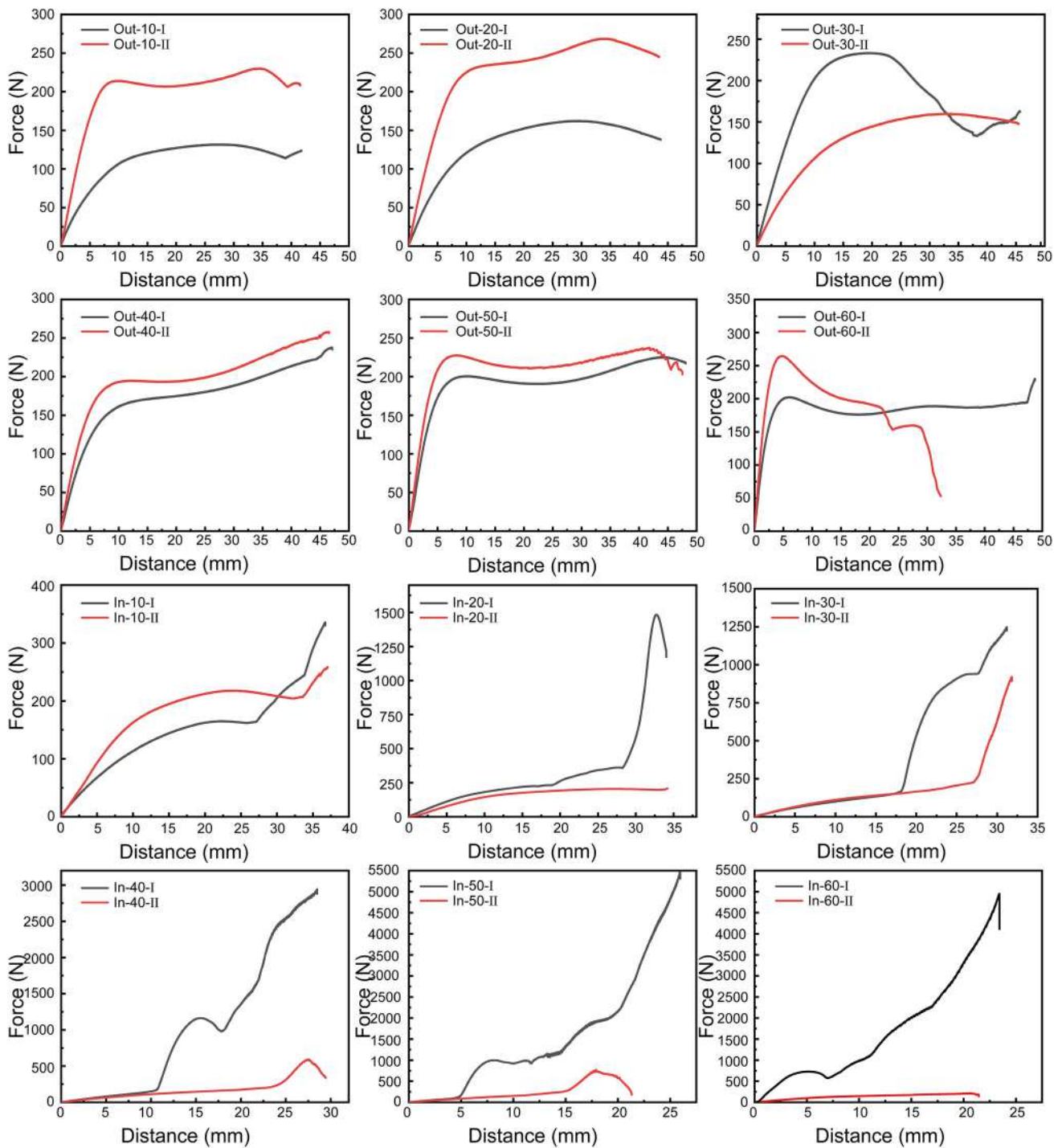
Fig. 9 Comparison of the load-bearing performance of thick-walled 3D kirigami-inspired honeycomb (TW3KH) structures before (I) and after (II) shape recovery

TW3KH structure is expected to be applied to space-saving load-bearing equipment.

Author contributions CBY conceived the idea, designed the experiments, carried out the data analysis, and wrote the first draft of the manuscript. WZ contributed to the guidance of the theoretical calculations and idea improvement. LWL contributed to supervision. FFL contributed to language modification. YJL and JSL had scientific discussions and improved the manuscript. All authors reviewed and commented on the manuscript.

Declarations

Conflict of interest The authors declare that they have no conflict of interest.

Ethical approval This article does not contain any studies with human or animal subjects performed by any of the authors.

References

1. Wang ZG (2019) Recent advances in novel metallic honeycomb structure. Compos Part B Eng 166:731–741. https://doi.org/10.1016/j.compositesb.2019.02.011
2. Morales MM, Ramos MJG, Vazquez PP et al (2020) Distribution of chemical residues in the beehive compartments and their transfer to the honeybee brood. Sci Total Environ 710:136288. https://doi.org/10.1016/j.scitotenv.2019.136288
3. Qi C, Jiang F, Yang S (2021) Advanced honeycomb designs for improving mechanical properties: a review. Compos Part B Eng 227:109393. https://doi.org/10.1016/j.compositesb.2021.109393
4. Zhang Q, Liu H (2020) On the dynamic response of porous functionally graded microbeam under moving load. Int J Eng Sci 153:103317. https://doi.org/10.1016/j.ijengsci.2020.103317
5. Zhang JJ, Lu GX, You Z (2020) Large deformation and energy absorption of additively manufactured auxetic materials and structures: a review. Compos Part B Eng 201:108340. https://doi.org/10.1016/j.compositesb.2020.108340
6. Zhao W, Yue CB, Liu LW et al (2023) Mechanical behavior analyses of 4D printed metamaterials structures. Compos Struct 304:116360. https://doi.org/10.1016/j.compstruct.2022.116360
7. Gao JY, You Z (2022) Origami-inspired Miura-ori honeycombs with a self-locking property. Thin-Walled Struct 171:108806. https://doi.org/10.1016/j.tws.2021.108806
8. Wang QS, Li ZH, Zhang Y et al (2020) Ultra-low density architectured metamaterial with superior mechanical properties and energy absorption capability. Compos Part B Eng 202:108379. https://doi.org/10.1016/j.compositesb.2020.108379
9. Bates SRG, Farrow IR, Trask RS (2019) Compressive behaviour of 3D printed thermoplastic polyurethane honeycombs with graded densities. Mater Des 162:130–142. https://doi.org/10.1016/j.matdes.2018.11.019
10. Bayle O, Lorenzoni L, Blancquaert T et al (2016) Exomars entry descent and landing demonstrator mission and design overview. ExoMars EDM Overv Pap NASA

11. Zhang YW, Yan LL, Zhang WB et al (2019) Metallic tube-reinforced aluminum honeycombs: compressive and bending performances. Compos Part B Eng 171:192–203. https://doi.org/10.1016/j.compositesb.2019.04.044
12. Zhao W, Li N, Liu LW et al (2022) Origami derived self-assembly stents fabricated via 4D printing. Compos Struct 293:115669. https://doi.org/10.1016/j.compstruct.2022.115669
13. Bai JB, Chen D, Xiong JJ et al (2019) Folding analysis for thin-walled deployable composite boom. Acta Astronaut 159:622–636. https://doi.org/10.1016/j.actaastro.2019.02.014
14. Zhao W, Huang ZP, Liu LW et al (2022) Bionic design and performance research of tracheal stent based on shape memory polycaprolactone. Compos Sci Technol 229:109671. https://doi.org/10.1016/j.compscitech.2022.109671
15. Xiao R, Feng XB, Fan R et al (2020) 3D printing of titanium-coated gradient composite lattices for lightweight mandibular prosthesis. Compos Part B Eng 193:108057. https://doi.org/10.1016/j.compositesb.2020.108057
16. Zhao W, Huang ZP, Liu LW et al (2021) Porous bone tissue scaffold concept based on shape memory PLA/Fe_3O_4. Compos Sci Technol 205:108563. https://doi.org/10.1016/j.compscitech.2020.108563
17. Zhao W, Zhu J, Liu LW et al (2021) Analysis of small-scale topology and macroscale mechanical properties of shape memory chiral-lattice metamaterials. Compos Struct 262:113569. https://doi.org/10.1016/j.compstruct.2021.113569
18. Zhao W, Zhang FH, Leng JS et al (2019) Personalized 4D printing of bioinspired tracheal scaffold concept based on magnetic stimulated shape memory composites. Compos Sci Technol 184:107866. https://doi.org/10.1016/j.compscitech.2019.107866
19. Zhao W, Liu LW, Zhang FH et al (2019) Shape memory polymers and their composites in biomedical applications. Mater Sci Eng C 97:864–883. https://doi.org/10.1016/j.msec.2018.12.054
20. Yue CB, Li M, Liu YT et al (2021) Three-dimensional printing of cellulose nanofibers reinforced PHB/PCL/Fe_3O_4 magneto-responsive shape memory polymer composites with excellent mechanical properties. Addit Manuf 46:102146. https://doi.org/10.1016/j.addma.2021.102146
21. Zhao W, Liu LW, Lan X et al (2023) Thermomechanical constitutive models of shape memory polymers and their composites. Appl Mech Rev 75(2):020802. https://doi.org/10.1115/1.4056131
22. Van Manen T, Janbaz S, Ganjian M et al (2020) Kirigami-enabled self-folding origami. Mater Today 32:59–67. https://doi.org/10.1016/j.mattod.2019.08.001
23. Castle T, Sussman DM, Tanis M et al (2016) Additive lattice kirigami. Sci Adv 2(9):e16012. https://doi.org/10.1126/sciadv.1601258
24. Ning X, Wang XJ, Zhang Y et al (2018) Assembly of advanced materials into 3D functional structures by methods inspired by origami and kirigami: a review. Adv Mater Interfaces 5(13):1800284. https://doi.org/10.1002/admi.201800284
25. Callens SJP, Zadpoor AA (2018) From flat sheets to curved geometries: origami and kirigami approaches. Mater Today 21(3):241–264. https://doi.org/10.1016/j.mattod.2017.10.004
26. Zhai ZR, Wu LL, Jiang HQ (2021) Mechanical metamaterials based on origami and kirigami. Appl Phys Rev 8(4):41319. https://doi.org/10.1063/5.0051088
27. Ma JY, Dai HP, Chai SB et al (2021) Energy absorption of sandwich structures with a kirigami-inspired pyramid foldcore under quasi-static compression and shear. Mater Des 206:109808. https://doi.org/10.1016/j.matdes.2021.109808
28. Zhang X, Ma JY, Li MY et al (2022) Kirigami-based metastructures with programmable multistability. Proc Natl Acad Sci USA 119(11):e2117649119. https://doi.org/10.1073/pnas.2117649119
29. Le DH, Xu Y, Tentzeris MM et al (2020) Transformation from 2D meta-pixel to 3D meta-pixel using auxetic kirigami for

programmable multifunctional electromagnetic response. Extrem Mech Lett 36:100670. https://doi.org/10.1016/j.eml.2020.100670

30. Gruber P, Häuplik S, Imhof B et al (2007) Deployable structures for a human lunar base. Acta Astronaut 61:484–495. https://doi.org/10.1016/j.actaastro.2007.01.055

31. Thesiya DA, Srinivas AR, Shukla P (2015) A novel lateral deployment mechanism for segmented mirror/solar panel of space telescope. J Astron Instrum 4:1550006. https://doi.org/10.1142/S2251171715500063

32. Sareh S, Rossiter J (2012) Kirigami artificial muscles with complex biologically inspired morphologies. Smart Mater Struct 22(1):14004. https://doi.org/10.1088/0964-1726/22/1/014004

33. Sun J, Scarpa F, Liu YJ et al (2015) Morphing thickness in airfoils using pneumatic flexible tubes and kirigami honeycomb. J Intell Mater Syst Struct 27(6):755–763. https://doi.org/10.1177/1045389X15580656

34. Zhang YH, Yan Z, Nan KW et al (2015) A mechanically driven form of kirigami as a route to 3D mesostructures in micro/nanomembranes. Proc Natl Acad Sci USA 112(38):11757–11764. https://doi.org/10.1073/pnas.1515602112

35. Tao R, Ji LT, Li Y et al (2020) 4D printed origami metamaterials with tunable compression twist behavior and stress-strain curves. Compos Part B Eng 201:108344. https://doi.org/10.1016/j.compositesb.2020.108344

36. Liu Y, Zhang W, Zhang FH et al (2018) Shape memory behavior and recovery force of 4D printed laminated Miura-origami structures subjected to compressive loading. Compos Part B Eng 153:233–242. https://doi.org/10.1016/j.compositesb.2018.07.053

37. Xin XZ, Liu LW, Liu YJ et al (2020) Origami-inspired self-deployment 4D printed honeycomb sandwich structure with large shape transformation. Smart Mater Struct 29(6):65015. https://doi.org/10.1088/1361-665x/ab85a4

38. Song C, Zou BH, Cui ZM et al (2021) Thermomechanically triggered reversible multi-transformability of a single material system by energy swapping and shape memory effects. Adv Funct Mater 31(32):2101395. https://doi.org/10.1002/adfm.202101395

39. Zhao W, Liu LW, Leng JS et al (2019) Thermo-mechanical behavior prediction of particulate reinforced shape memory polymer composite. Compos Part B Eng 179:107455. https://doi.org/10.1016/j.compositesb.2019.107455

40. Xin XZ, Liu LW, Liu YJ et al (2020) 4D printing auxetic metamaterials with tunable, programmable, and reconfigurable mechanical properties. Adv Funct Mater 30(43):2004226. https://doi.org/10.1002/adfm.202004226